Measurements in Situ and Spectral Analysis of Wind Flow Effects on Overhead Transmission Lines

Maciej Dutkiewicz[1,*] and Marcela R. Machado[2]

[1]UTP University of Science and Technology, Bydgoszcz, 85-796, Poland.
[2]University of Brasilia, Brasilia, 70910-900, Brazil.
[*]Corresponding Author: Maciej Dutkiewicz. Email: macdut@utp.edu.pl.

Abstract: In the paper an important issue of vibrations of the transmission line in real conditions was analyzed. Such research was carried out by the authors of this paper taking into account the cross-section of the cable being in use on the transmission line. Analysis was performed for the modern ACSR high voltage transmission line with span of 213.0 m. The purpose of the investigation was to analyze the vibrations of the power transmission line in the natural environment and compare with the results obtained in the numerical simulations. Analysis was performed for natural and wind excited vibrations. The numerical model was made using the Spectral Element Method. In the spectral model, for various parameters of stiffness, damping and tension force, the system response was checked and compared with the results of the accelerations obtained in the situ measurements. A frequency response functions (FRF) were calculated. The credibility of the model was assessed through a validation process carried out by comparing graphical plots of FRF functions and numerical values expressing differences in acceleration amplitude (MSG), phase angle differences (PSG) and differences in acceleration and phase angle total (CSG) values. Particular attention was paid to the hysteretic damping analysis. Sensitivity of the wave number was performed for changing of the tension force and section area of the cable. The next aspect constituting the purpose of this paper was to present the wide possibilities of modelling and simulation of slender conductors using the Spectral Element Method. The obtained results show very good accuracy in the range of both experimental measurements as well as simulation analysis. The paper emphasizes the ease with which the sensitivity of the conductor and its response to changes in density of spectral mesh division, cable cross-section, tensile strength or material damping can be studied.

Keywords: Transmission line; Spectral Element Method; frequency response function

1 Introduction

The rapid development of technology causes that modern construction objects have high strength parameters with low structural stiffness and low damping coefficient. These objects are particularly susceptible to dynamic load such as wind. Such structures include among others: tall buildings, chimneys, masts, suspended and cable stayed bridges and overhead transmission lines.

Overhead transmission lines are constantly subjected to variable wind loads which may gradually lead to the impairment of their durability, resulting in the shortened service life. That is the huge need to design and construct the overhead transmission lines with the respect of wide range of load cases acting on these slender structures. This is very important to develop the easy and fast methodology for design, taking into consideration all loads and uncertainties. Nowadays we see the wide development of new materials and solutions to raise the conductivity but at the same time we observe that conductors'

durability is change and require the permanent update analysis. Spectral Element Method seems to be such fast and easy tool which fulfills these requirements.

There are some theoretical and experimental researches on overhead transmission lines [1-5]. Wind forces cause three main types of conductor vibrations: Aeolian vibrations with a frequency from 3 to 150 Hz and amplitudes lower than the conductor diameter, galloping with a frequency from 0.1 to 1 Hz and amplitudes from ± 0.1 to 1 of conductor sag, wake induced vibrations with a frequency from 0.15 to 10 Hz and amplitudes from 0.5 to 80 times the conductor diameter [6-9].

The majority of common wind induced vibrations are Aeolian vibrations. These vibrations are generated as a result of vortices shed in the conductor wake under sustained wind of low speed from 1 to 7 m/s-they occur mainly in the vertical plane [7]. Vibrations of conductors both single and in a bundle, form standing waves with forced nodes and intermediate nodes located along the span at intervals depending on the frequency of free vibrations. When the conductor wind flow is laminar, alternately shedding vortices are formed in two points of the suction zone and make the conductor move perpendicularly towards the wind direction. The alternate shedding of vortices is regular. As a result, a so-called Karman vortex street is formed. When the frequency of the shedding of vortices is approximately equal to one of the frequencies of free vibrations of a conductor, a 'lock-in' phenomenon occurs. During this frequency synchronization, the conductor is in the resonance state. Aeolian vibrations occur on single conductors and conductors in a bundle. Although these vibrations are hardly noticeable due to low amplitude values (lower than the conductor diameter), they are very important, since they can lead to fatigue destruction of a conductor in points of high stress concentrations.

Galloping is an aero elastic self-excitation phenomenon characterized by low frequencies and high amplitudes, and it refers to single conductors and conductors in a bundle, with one or two loops of standing and running waves, or their combination in a conductor span. Standing waves may have one or more loops (up to 10) over the span length. However, a small number of loops are predominant. In most cases, galloping is caused by sustained wind of an average and high speed (V > 15 m/s), blowing on an asymmetrically loaded (e.g., with ice or wet snow) conductor. High amplitudes are observed in the vertical plane, whereas the frequencies depend on the type of a conductor and vibrations [4,10]. Galloping is a typical instability caused by the coupling of aerodynamic forces which affect the conductor with its vibrations. Conductor vibrations change the wind angle of attack on a periodic basis. The change of the angle of attack results in a change of aerodynamic forces affecting the conductor, which consequently changes the conductor response. The first, simplified criterion (if a single degree-of-freedom system is applied) pertaining to the instability connected with galloping was presented by Den Hartog [42] and developed by other researchers [10]. A precondition for galloping (on the basis of the quasi-steady theory) is the presence of negative aero elastic damping in the system. A conductor of a circular section cannot gallop due to its geometrical symmetry (dCL/dα = 0), unless this section is changed. Icing of a conductor changes its cross-section, thus it leads to its aerodynamic instability [10]. Research works carried out by Den Hartog indicate that the aerodynamic instability is the main reason for the galloping phenomenon. His research was conducted with an assumption that the vertical motion of a conductor is predominant, and the effect of torsion and horizontal motions can be ignored. Further research proved that the torsion motion is an integral part of the galloping phenomenon. The effect of a coupled torsion-translational motion plays a crucial role in most cases of progressing galloping [11].

These extremely important phenomena described above have mobilized the authors of the article to look for transmission line vibration solutions using numerical methods. Spectral Element Method (SEM) proved to be such a method. SEM is a meshing method similar to Finite Element Method (FEM), where the approximated element shape functions are substituted by exact dynamic shape functions obtained from the exact solution of governing differential equations. Therefore, a single element is sufficient to model any continuous and uniform part of the structure. This feature reduces significantly the number of elements required in the structure model and improves the accuracy of the dynamic system solution. At the same time, there are some drawbacks like the unavailability of exact wave solutions for most complex and 2D and 3D structures. In these cases, approximated spectral element modelling can be used and may

still provide very accurate solutions. Although SEM ensures exact frequency-domain it is not true for time-domain solutions, because errors due to aliasing or leakage are inevitable in the use of the inverse-DFT process. Thus, special attention in obtaining the inverse-DFT is required. In recent years some researchers were performed with use of SEM. The extensive study of the fundamentals and a variety of new applications such as composite laminated, periodic lattice, damage detection was presented in [12]. The wave behavior in composites and inhomogeneous media is studied in [13]. Studies related to structural damage detection have been developed in [14]. Other works using wave propagation and SEM to detect damage under the presence of structural randomness can also be found in references [15-17].

2 Mathematical Model of Overhead Transmission Line

Considering a simplified cable model, as shown in Fig. 1, the governing differential equation for the undamped free vibration is given by Clough and Yu [18-19]:

$$EI\frac{\partial^4 v}{\partial x^4} - T\frac{\partial^2 v}{\partial x^2} + \rho A\frac{\partial^2 v(x,t)}{\partial t^2} = 0 \tag{1}$$
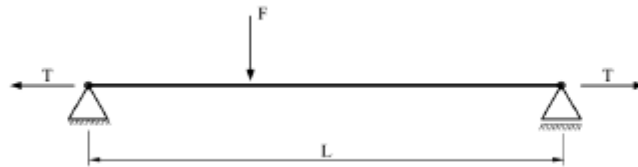

Figure 1: Analysed model

For a simply supported beam under axial force the natural frequency can be written as [20]:

$$\omega_n = \frac{\pi^2}{L^2}\sqrt{\frac{EI}{\rho A}}\left(n^4 + \frac{n^2 T L^2}{\pi^2 EI}\right)^{\frac{1}{2}}, \quad n = 1,2,\dots \tag{2}$$

where ρA is mass per unit length, EI the uniform bending rigidity, L is cable length, T is tension force, and $v(x,t)$ is the cable displacement as a function of the position x and time t.

The undamped Euler-Bernoulli beam equation of motion subjected to axial force and under bending vibration is governing by Eq. (1). Fig. 2 shows an elastic two-node element with a uniform rectangular cross-section subjected to an axial force, where the properties are assumed to be deterministic variables. A structural internal damping is introduced into the beam formulation by adding into Young's modulus weighted by a complex damping factor $i\eta, i = \sqrt{-1}, \eta$ is the hysteretic structural loss factor, to obtain $E = E(1 + i\eta)$.
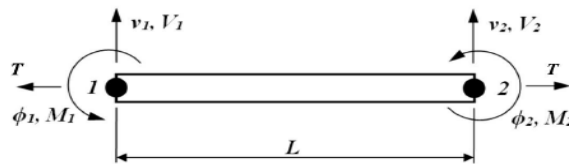

Figure 2: Two-node spectral element

By considering a constant coefficient a displacement solution can be assumed of the form [21-22]:

$$v(x,t) = v_0 e^{-i(kx-\omega t)} \tag{3}$$

where v_0 is a amplitude, ω is the frequency and k is the wave number. Substituting it at Eq. (1), the dispersion equation is given by:

$$k^4 EI + k^2 T - \omega^2 \rho A = 0 \tag{4}$$

There are two distinct wave modes in the positive direction (k^2), which is positive-going waves with wave numbers given as

$$k_1 = \sqrt{-\frac{T}{2EI} + \sqrt{\left(\frac{T}{2EI}\right)^2 + \frac{\rho A \omega^2}{EI}}} \tag{5}$$

$$k_2 = -\sqrt{-\frac{T}{2EI} - \sqrt{\left(\frac{T}{2EI}\right)^2 + \frac{\rho A \omega^2}{EI}}} \tag{6}$$

The general solution for the Euler-Bernoulli beam spectral element subjected to axial load of length L, can be expressed in the form:

$$v(x,\omega) = a_1 e^{-ikx} + a_2 e^{-kx} + a_3 e^{-ik(L-x)} + \tag{7}$$
$$+ a_4 e^{-k(L-x)} = s(x,\omega)a$$

where

$$s(x,\omega) = \left\{ e^{-ikx}, e^{-kx}, e^{-ik(L-x)}, e^{-k(L-x)} \right\} \tag{8}$$

$$a(x,\omega) = \{a_1, a_2, a_3, a_4\}^T$$
$$\tag{9}$$

The spectral nodal displacements and slopes of the beam element are related to the displacement field at node 1 (x=0) and node 2 (x=L), by

$$\mathbf{d} = \begin{bmatrix} v_1 \\ \phi_2 \\ v_2 \\ \phi_2 \end{bmatrix} = \begin{bmatrix} v(0) \\ v'(0) \\ v(L) \\ v'(L) \end{bmatrix} \tag{10}$$

By substituting Eq. (7) into the right-hand side of Eq. (10) and written in a matrix form gives

$$\mathbf{d} = \begin{bmatrix} s(0,\omega) \\ s'(0,\omega) \\ s(L,\omega) \\ s'(L,\omega) \end{bmatrix} a = G(\omega)a \tag{11}$$

where

$$G(\omega) = \begin{bmatrix} 1 & 1 & e^{-ikL} & e^{-kL} \\ -ik & -k & ike^{-ikL} & ke^{-kL} \\ e^{-ikL} & e^{-kL} & 1 & 1 \\ -ike^{-ikL} & -ke^{-kL} & ik & k \end{bmatrix} \tag{12}$$

The frequency-dependent displacement within an element is interpolated from the nodal displacement vector $\mathbf{d}$, by eliminating the constant vector a from Eq. (7) and using Eq. (11), it is expressed as:

$$v(x,\omega) = g(x,\omega)d \tag{13}$$

where the shape function is

$$g(x,\omega) = s(x,\omega)G^{-1}(\omega) = s(x,\omega)\Gamma(\omega) \tag{14}$$

The dynamic stiffness matrix for the spectral beam element under axial tension can be determined as:

$$S(\omega) = K(\omega) - \omega^2 M(\omega) \tag{15}$$

where

$$\boldsymbol{K}(\omega) = \int_0^L \left(EI\boldsymbol{g}''(x)^T \boldsymbol{g}''(x) + T\boldsymbol{g}'(x)^T \boldsymbol{g}'(x) \right) dx \tag{16}$$

$$\boldsymbol{M}(\omega) = \rho A \int_0^L \boldsymbol{g}(x)^T \boldsymbol{g}(x) d\boldsymbol{x} \tag{17}$$

where ' express the spatial partial derivative. By solving the integral, the dynamic stiffness matrix is:

$$\boldsymbol{S}(\omega) = \frac{EI}{\Delta} \begin{bmatrix} s_{11} & s_{12} & s_{13} & s_{14} \\ & s_{22} & s_{23} & s_{24} \\ & & s_{33} & s_{34} \\ sym & & & s_{44} \end{bmatrix} \tag{18}$$

where $\Delta = \cos(\mathrm{k} \, \mathrm{L})\cosh(\mathrm{k} \, \mathrm{L}) - 1$ and the components of element matrix (Eq. (18)) are given as

$$s_{11} = -k^3(cos(kL)sinh\,(kL) + sin(kL)cosh(kL))$$

$$s_{12} = -k^2 sin\,(kL)sinh\,(kL)$$
$$s_{13} = k^3\,(sin\,(kL) + sinh\,(kL))$$
$$s_{14} = k^2\,(cos(kL) - cosh(kL))$$
$$s_{22} = k(cos(kL)sinh(kL) - sin(kL)\,cosh(kL)) \tag{19}$$
$$s_{23} = k^2(cosh(kL) - cos(kL))$$
$$s_{24} = k(sin\,(kL) - sinh(kL))$$
$$s_{33} = -k^3(cos(kL)sinh(kL) + sin(kL)cosh(kL))$$
$$s_{34} = k^2\,sin(kL)\,sinh(kL)$$
$$s_{44} = k(cos(kL)\,sinh(kL) - sin(kL)\,cosh(kL))$$

As far as structure beam is uniform without any sources of discontinuity, it can be represented by a single spectral element with very accurate solutions [23]. However, if there exist sources of discontinuity such as the point loads the beam should be spatially discretized into spectral elements. Analogous to Finite Element Method (FEM) [24], the spectral elements can be assembled to form a global structure matrix system [12]

3 Validation and Verification

The article presents a validation analysis in relation to the measurement and the simulation model.

The essence of using computer simulation methods requires determining their level of accuracy in relation to direct measurement of the actual model. The required level of accuracy of the simulation depends on the purposes for which the simulation is applied. According to AIAA and ASME [25-26] validation and verification are the basic tools used to determine the credibility of the used model. Validation explains how the model represents reality, while verification determines that the implementation of the model properly represents the adopted description and solutions of the model application. In the validation process, the accuracy is referred to the measurement results, in verification the accuracy is referred to the pattern obtained in the calculation model. Uncertainty and error are the reasons that affect the accuracy of results obtained in the modelling and simulation process. Uncertainty results from the lack of knowledge or incomplete knowledge about the physical characteristics, the analyzed parameter, wrong assumptions concerning, for example, the flow of wind around the analyzed body with different surface porosity, may result from the complexity of the phenomenon, e.g., wind turbulence. Errors can be classified as confirmed and unconfirmed (conscious and unconscious). Errors in rounding are confirmed errors, while programming errors are not anomalous errors. The validation strategy is to identify and quantify errors and uncertainties in the conceptual and computational model.

The strategy of model verification is connected with the identification and quantification of errors consisting in obtaining inappropriate convergence of spatial and temporal discretization, convergence of iterations and computer programming. The essence of verification consists in a detailed analysis of the size of the division grid and the time step. With the size of the grid size and the time step approaching zero, the discretization error should asymptotically reach zero.

Validation metrics is the subject of interest of many researchers. Oberkampf and Trucano [27] present an extensive review of the literature in validation and verification (V&V) in computational fluid dynamics (CFD), discusses methods and procedures for assessing V&V, and develops a number of extensions to existing ideas. The review of the development of V&V terminology and methodology points out the contributions from members of the operations research, statistics, and CFD communities. Authors explain that the fundamental strategy of verification is the identification and quantification of errors in the computational model and its solution. A set of guidelines is proposed for designing and conducting validation experiments, supported by an explanation of how validation experiments are different from traditional experiments and testing. A description is given of a relatively new procedure for estimating experimental uncertainty that has proven more effective at estimating random and correlated bias errors in wind-tunnel experiments than traditional methods.

Aeschliman, Oberkampf and Blottner [28] describe a methodology for verification, calibration, and validation (VCV). A novel approach to uncertainty analysis is described which can both distinguish between and quantify various types of experimental error, and whose attributes are used to help define an appropriate experimental design for code VCV experiments.

Schwer [29] presents developed metrics and their wave form comparative quantification was demonstrated through application to analytical wave forms, measured and computed free-field velocity histories, and comparison with Subject Matter Expert opinion.

William, Oberkampf and Smith [30] propose a framework for assessing validation experiments for computational fluid dynamics regarding information content, data completeness, and uncertainty quantification. This framework combines two concepts: the concept of a strong-sense benchmark for validation experiments and the modelling assessment procedure referred to as the predictive capability maturity method. The validation experiment assessment requirements are captured in a table of attributes: Experimental Facility, Analog Instrumentation and Signal Processing, Boundary and Initial Conditions, Fluid and Material Properties, Test Conditions, and Measurement of System Responses and four levels of information completeness for each attribute.

William, Oberkampf and Barone [31] develop a validation metric that is based on the statistical concept of confidence intervals. Using this fundamental concept, two specific metrics: one that requires interpolation of experimental data and one that requires regression (curve fitting) of experimental data. Authors discuss how the present metrics are easily interpretable for assessing computational model accuracy, as well as the impact of experimental measurement uncertainty on the accuracy assessment.

Russell [32] develops a new set of magnitude, phase, and comprehensive error measures to evaluate the differences between two functions or test and analytical data. The error factors are on the same relative scale and have physical interpretations.

Geers [33] presents the metric for comparing calculated transient response history with its measured counterpart. The proposed measure assigns a single numerical value to the discrepancy between the two histories over a specified comparison period. Computational of the measure involves the integration in time of squares and products of the calculated and measured histories. Representative results are shown for both idealized and actual response histories.

Validation metrics problems were developed also in works [34-41].

In the present paper the formulation of the validation metrics is proposed as follows [29,41]:

$$\vartheta_{mm} = (t_2 - t_1)^{-1} \int_{t_1}^{t_2} m^2(t)dt \qquad (20)$$

$$\vartheta_{cc} = (t_2 - t_1)^{-1} \int_{t_1}^{t_2} c^2(t)dt \qquad (21)$$

$$\vartheta_{mc} = (t_2 - t_1)^{-1} \int_{t_1}^{t_2} m(t)c(t)dt \qquad (22)$$

where $m(t)$ is the measured history and $c(t)$ is the simulation history, $t_1 < t < t_2$ is the time span of interest for the response history. The amplitude validation metric (AVM) is:

$$M_{SG} = \sqrt{\frac{\vartheta_{cc}}{\vartheta_{mm}}} - 1 \qquad (23)$$

The AVM is insensitive to phase discrepancies and is based upon the area under the squared response history. The phase validation metric (PVM) is:

$$P = \frac{1}{\pi} acos\left(\frac{\vartheta_{mc}}{\sqrt{\vartheta_{mm}\vartheta_{cc}}}\right) \qquad (24)$$

PVM is insensitive to magnitude differences. The comprehensive validation metric is:

$$C_{SG} = \sqrt{M_{SG}^2 + P^2} \qquad (25)$$

In this paper, another approach proposed by Oberkampf, Trucano [27] is taken into the consideration:

$$V = 1 - \frac{1}{I}\sum_{i=1}^{i=I} tanh\left|\frac{c(t) - m(t)}{m(t)}\right| \qquad (26)$$

This type of metric has the following advantages [27]. First, it normalizes the difference between the computational results and the experimental data. Thus a relative error norm is computed. This normalization, however, is inappropriate when any of the $m(t)$ are near zero. When the difference between the computational results and the experimental data is zero at all measurement locations, then the validation metric is unity, i.e., perfect agreement between the computational results and the experimental data. When the summation of the relative error becomes large, the validation metric approaches zero.

In the article, the validation process consisted in determining the validation coefficients and checking whether these coefficients are smaller than the assumed level of 30% in full range of analysed domain [33]. Checks were carried out for different stiffness and tension values within the fixed time range. In the work, the verification process was carried out for different grid densities-spectral element's length.

4 Results from Measurements in Situ and Numerical Analysis

Experiments were performed in situ, during the maintenance period of the transmission line. The conductor was aluminium conductor steel reinforced type (ACSR), and according to technical data sheet it had weight per unit length m = 0.974 kg/m and nominal diameter D = 21.7 mm. The span length of the conductor was 213 m. The elasticity module was E = 77 GPa, density ρ = 2700 kg/m³.

Transmission line was located at height of 30 m above the ground, mounted to the steel towers. Conditions of the measurements was as follows: temperature of the air was 11 degrees of Celsius, measured wind speed during the measurement time was in the range of 0.0 to 10.5 m/s. Measurements of accelerations were performed in the mid span of 106.5 m Fig. 3. Wind speed was measured with the anemometer and vibrations with accelerometers manufactured by Bruel & Kjaer. Signals from the piezoelectric

accelerometers were read and recorded by Pulse acquisition data system from Bruel & Kjaer. Natural vibrations were measured. Records from the measurements of natural vibrations are presented in Fig. 4.

(a)   (b)

Figure 3: Experiments in situ, (a) view of the overhead transmission line (b) accelerometers mounted to the transmission conductor

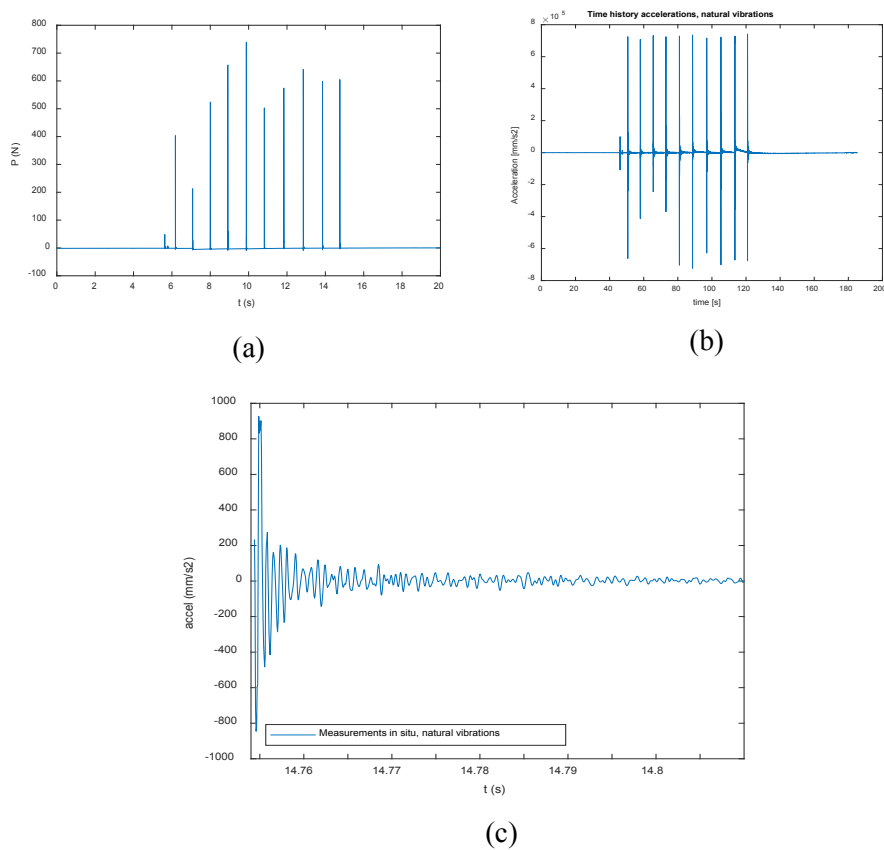(a)   (b)

(c)

Figure 4: Force signal, (a) impulse force signal, (b) full acceleration record of cable's response (c) last part acceleration record of cable's response

Modal hammer was used for generation of impulse forces. For each case of natural and excited vibrations, the frequency band [0,50] was taken into consideration as shown in Tab. 1.

Table 1: Parameters of records for measurements in situ

Excitation	Frequency band [Hz]	Time range [s], $[t_0, t_e]$	Sampling frequency, f_s [Hz]	Accelerometers
Impulse force	[0, 50]	[0, 90]	512	Acc1 and Acc2
Wind action	[0, 50]	[0, 90]	512	Acc1 and Acc2

4.1 Natural Vibrations

On the basis of the formulas presented in Eqs. (15-17), it is possible to obtain the Frequency Response Function (FRF) of the overhead transmission conductor. For the numerical tests, it is assumed a pinned-pinned boundary condition.

In the beginning, in order to verify the proposed model, the 10 firsts resonance picks of the FRF are compared with the natural frequency analytical formulation (Eq. (2)) and with the results received from the measurements and numerical simulations. Once, the structure is excited with a unitary force we can expect that the resonance picks are close to the natural frequency of the system. Fig. 5 shows the FRF for experimental data and simulations measured at point $L_1 = 33$ m from the node. For the purpose of the numerical simulation it was assumed the circular area of the conductor $A = 108$ mm^2 and $A = 223.7$ mm^2 and tension force of $T = 30$ kN. Figs. 5(a)-5(b) shows the comparison of experiments and best fit simulation functions. The zoom image at 0 to 5 Hz frequency band to better visualization of the firsts resonance pick is shown on Fig. 5(b). Tab. 2 summarized the 10-first's analytical natural frequency and resonance pick obtained with the SEM model and from measurements in situ.
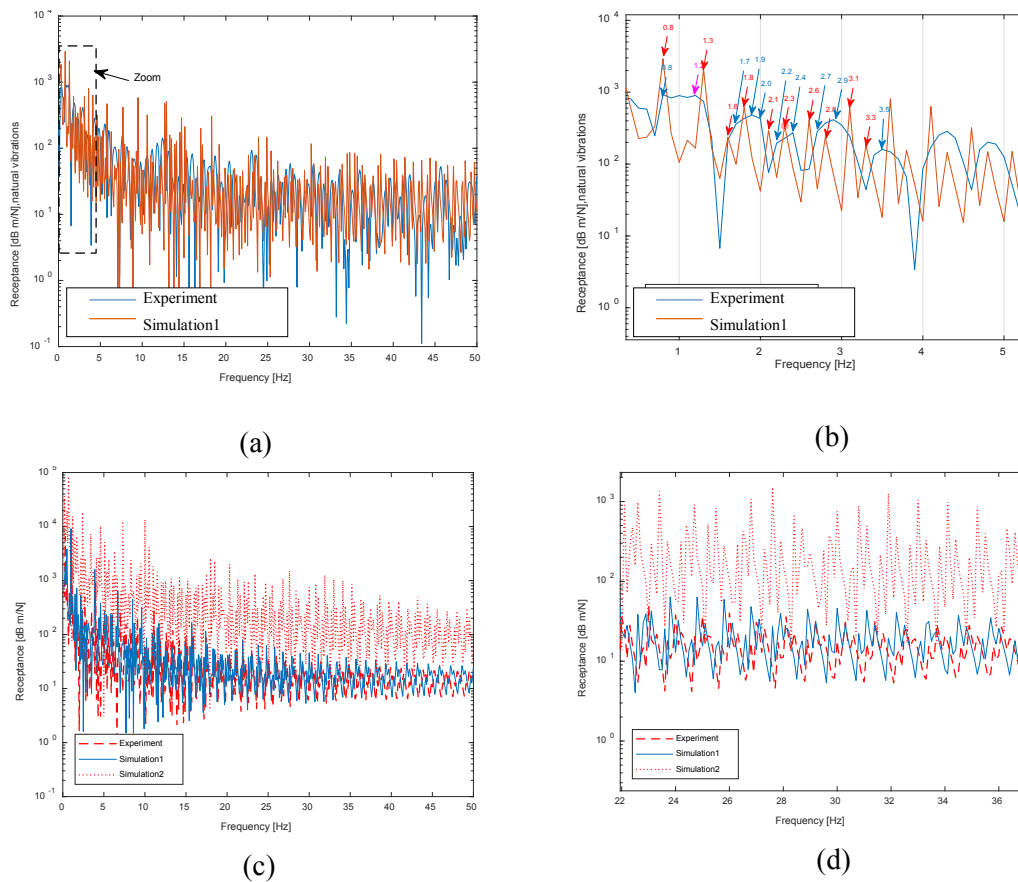

(a)   (b)

(c)   (d)

Figure 5: FRF measured in situ and from the spectral model, (a) FRF from experiment and simulation1 for $A = 223.7$ mm^2, tension force $T = 30$ kN, (b) zoom image in 0 to 5 Hsz frequency band for experiment

and simulation1 results, (c) comparison of experiment, simulation1 (A = 223.7 mm²) and simulation2 (A = 108 mm²), tension force T = 30 kN, (d) zoom image in 22 to 36 Hz frequency band for experiment, simulation1, simulation2 results

Table 2: Comparison between 10 firsts analytical natural frequency with resonance picks obtained in the experiment and simulation1 (A = 223.7mm², T = 30 kN)

ω_n (Hz)	0.366	0.733	1.1	1.468	1.837	2.206	2.578	2.950	3.325	3.701
Simulation1	0.8	1.3	1.6	1.8	2.1	2.3	2.6	2.8	3.1	3.3
Experiment	0.8	1.2	1.7	1.9	2.0	2.4	2.7	2.9	-	3.5

4.2 Wind Vibrations

In the spectral analysis the wind force acting on the overhead transmission line is determined by the expression:

$$F = \frac{1}{2}\rho V^2 DLC \tag{27}$$

where $\rho = 1.25 \, kg/m^3$, V is the wind speed, D is the diameter of the transmission line, L is the length of the line, C is the aerodynamic coefficient, equal to 2. The wind speed that most fit the response of overhead transmission line is shown on Fig. 6. The results of analysis in Fig. 7 present two curves received in spectral analysis and analysis is from measurements in situ. In the range of frequency (0,20) Hz, the amplitudes from spectral analysis are higher than from measurements in situ.
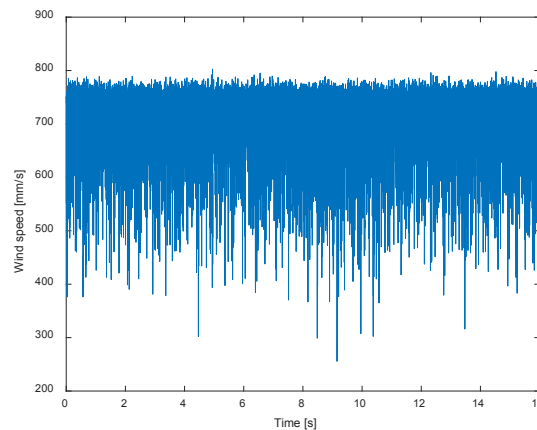

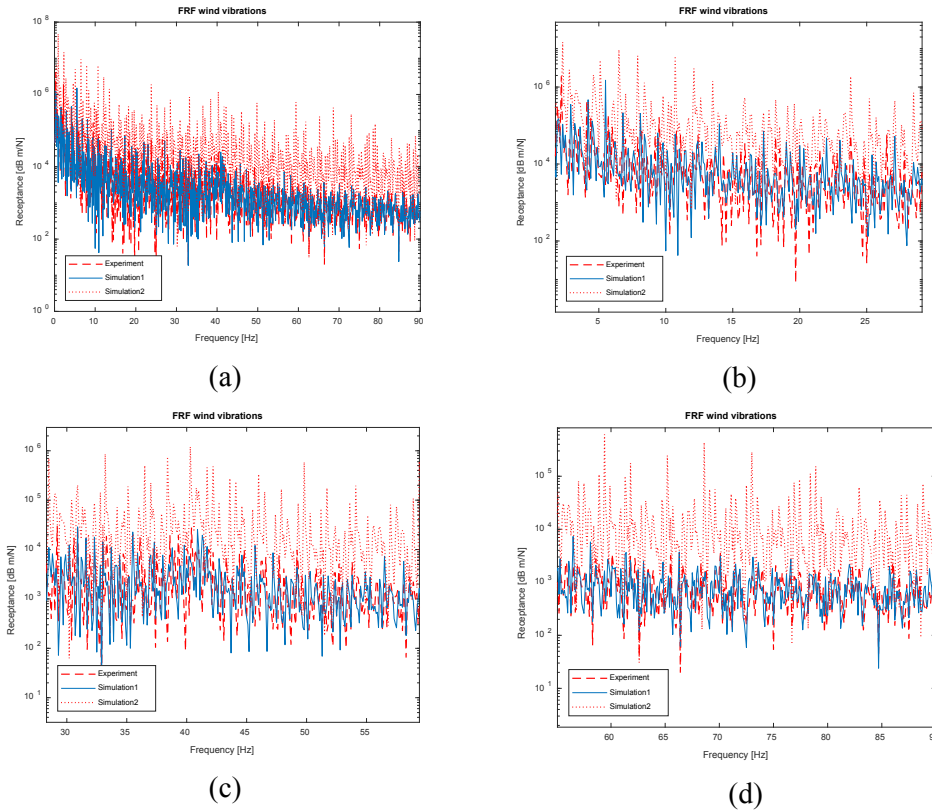**Figure 6:** Wind speed signal used for spectral analysis

(a)   (b)

(c)   (d)

Figure 7: FRF for experiment and simulation, (a) simulation 1 for A = 223.7 mm^2, tension force T = 30 kN, simulations2 for A = 108 mm^2, tension force T = 30 kN, (b) zoom image in 5 to 25 Hz frequency band, (c) zoom image in 30 to 55 Hz frequency band, (d) zoom image in 60 to 90 Hz frequency band

For the analysis of natural vibrations, the use of spectral elements length L_1 = 21.3 m results the amplitude validation metric AVM = 0.02801, for L_1 = 53.25 m the AVM = 0,007723. Selected results of analyzes validation metrics are presented in Tab. 3 for different spectral element length and in Tab. 4 for different cable section area. The analysis shows the slight impact of changes of phase validation metric (PVM) along with the change in the division of the density of the spectral elements and changes in the cable cross-section.

Table 3: Validation metrics for different spectral element length

	Natural vibrations			Wind vibrations		
L_1 , [m]	M_{SG}	P	C_{SG}	M_{SG}	P	C_{SG}
21.30	0,0280	0,1609	0,1633	0,1301	0,1716	0,2153
53.25	0,0077	0,1580	0,1582	0,0097	0,1682	0,1685
71.00	0,0701	0,1651	0,1794	0,0025	0,1671	0,1671

Table 4: Validation metrics for different cable section area

	Natural vibrations			Wind vibrations		
A, [m^2]	M_{SG}	P	C_{SG}	M_{SG}	P	C_{SG}
223.70	0,0002	0,1435	0,1554	0,2115	0,0097	0,1682
240.00	0,0002	0,0077	0,1580	0,1582	0,2335	0,1704
264.45	0,0003	0,3436	0,1544	0,3767	0,4650	0,1684

Figs. 8 and 9 present the results of the validation metrics analysis according with formulas Eqs. (20)-(26) described in Section 3 of this paper in the full range of time domain records, $[t_0, t_e] = [0, 90]$.
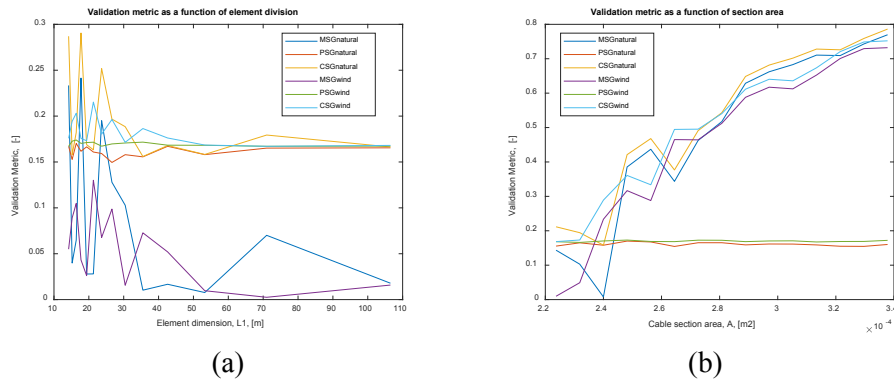

(a)   (b)

Figure 8: Validation metric: (a) as the function of the element division; (b) as the function of cable section area

Fig. 9 presents the dependence of relative error and validation metric in formulation of Eq. (26).
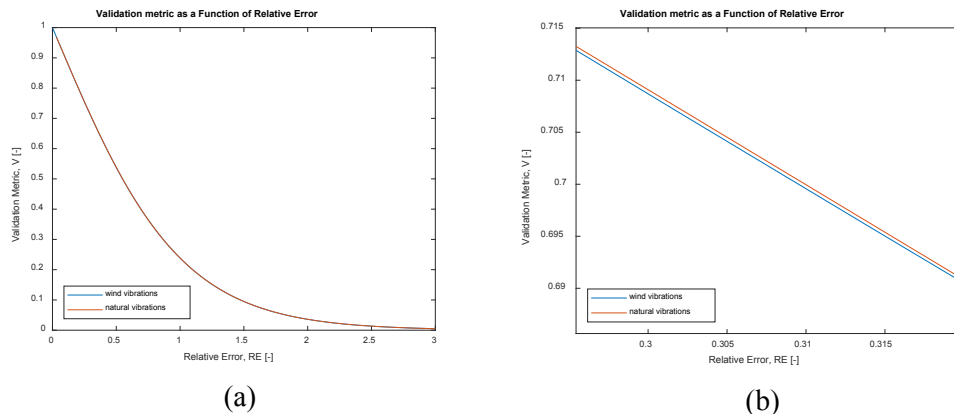

(a)   (b)

Figure 9: Validation metric as a function of the relative error for the wind and natural vibrations before fitting the functions: (a) full range; (b) zoom in the range of the 0.2 to 0.32

Fig. 10 presents the sensitivity of hysteretic damping on changes of tension force and section area of the conductor. Hysteretic damping is expressed by the wave number described by the Eqs. (5)-(6).

(a)   (b)
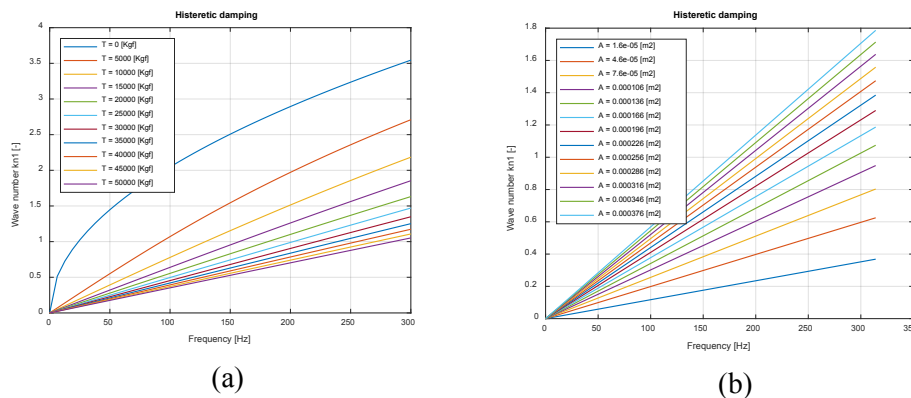
Figures 10: Hysteretic damping for the conductor: (a) change of tension force; (b) change of section area

5 Conclusions

In the paper the vibrations of the power transmission line in the natural environment and comparison with the results obtained in the numerical analysis was performed. Experimental tests were carried out on the currently operating modern ACSR high voltage transmission line with the span of 213.0 m. The natural working conditions of the cable were determined by the action of wind in the range from 0.0 to 10.5 m/s. The numerical model was made using the Spectral Element Method. Experimental data from measurements was used in the estimation process and frequency response functions were created and compared for experiment and simulation results.

In the spectral model, for various parameters of stiffness, damping and tension force, the system response was checked and compared to the results of the vibration accelerations obtained in the situ measurement. The frequency analysis was carried out. The credibility of the model was assessed through a validation process carried out by comparing graphical plots of FRF functions and numerical values expressing differences in acceleration amplitude (MSG), phase angle differences (PSG) and differences in acceleration and phase angle total (CSG) values. Furthermore, particular attention was paid to the hysteretic damping analysis. Sensitivity of the wave number was performed for changing of the tension force and section area of the cable.

The next aspect constituting the purpose of this article was to present the wide possibilities of modelling and simulation of slender conductors using the Spectral Element Method. The obtained results show very good accuracy in the range of both experimental measurements as well as simulations analysis. The paper emphasizes the ease with which the sensitivity of the cable and its response to changes in density of spectral mesh division, cable cross-section, tensile strength or material damping can be studied.

In the paper, a very important issue of vibration of the actual transmission line was performed. In the literature, there are not too many studies on modern constructions of high-voltage transmission lines under real working conditions. Such research was carried out by the authors of this paper, taking into account the modern cross-section of the cable currently in use on the transmission line. It is worth noting that the presented results bring closer the producers an users of power transmission lines for the application of more durable cables than those currently used and more resistant to fatigue damage being the main cause of cable breakages and transmission infrastructure.

References

1. Dutkiewicz, M. (2017). Experimental measurements of dynamical wind load acting on the overhead transmission line. *Anul XXIV, 1,* 88-100.
2. Vecchiarelli, J., Curie, I. G., Havard, D. G. (2000). Computational analysis of aeolian conductor vibration with a stockbridge-type damper. *Journal of Fluids and Structures, 14,* 489-509.
3. Meynen, H., Verma, P., Hagedorn, P., Schafer, M. (2005). On the numerical simulation of vortex-induced vibrations of oscillating conductors. *Journal of Fluids and Structures, 21(1).*
4. Gołębiowska, I., Dutkiewicz, M., Usewicz, B. (2015). Methods of damping of overhead transmission lines. *TTS, 12(5),* 2544-2548.
5. Wang, H. Q., Miao, J. C., Luo, J. H., Huang, F., Wang, L. G. (1997). The free vibration of long-span transmission line conductors with dampers. *Journal of Sound and Vibr, 208(4),* 501.
6. Gołębiowska, I., Dutkiewicz, M. (2016). The effectiveness of vibration damper attached to the cable due to wind action. *EPJ Web of Conferences,143,* 02029.
7. Dutkiewicz, M. (2017). Interaction of bridge cables and wake behind in the vortex induced vibrations, *14th International Conference Dynamical Systems-Theory and Application*s, Łódź, Poland.
8. Gołębiowska, I., Dutkiewicz, M. (2017). Vortex induced vibration and wind flow around bridge cables. *Proceedings of 14th International Conference on Acoustics and Vibration of Mechanical Structures,* 307-314.
9. Gołębiowska, I., Dutkiewicz, M. (2017). Analysis of wind flow around the bridge cable. *IOP Conference Series: Materials Science and Engineering, 245, 032066.*
10. Gołębiowska, I., Dutkiewicz, M. (2018). Galloping of overhead power lines conductors. *Proceedings of 24th*

International Conference on Engineering Mechanics, 257-260.

11. Luongo, A., Zulli, D., Piccardo, G. (2009). On the effect of twist angle on nonlinear galloping of suspended cables. *Computers and Structures, 87(15-16),* 1003-1014.

12. Lee, U. (2009). Spectral Element Method in structural dynamics. *Wiley & Sons*, Singapore.

13. Gopalakrishnan, S., Chakraborty, A, Mahapatra, D. R. (2007). Spectral finite element method. *Springer Verlag*, New York.

14. Fabro, A. T., Ritto, T. G., Sampaio, R., Arruda, J. R. F. (2010). Stochastic analysis of a cracked rod modeled via the Spectral Element Method, *Mechanics Research Communications, 37,* 326-331.

15. Flynn, E. B., Todd, M., Croxford, J., Drinkwater, B., Wilcox, P. (2011). Enhanced detection through low order stochastic modeling for guided-wave structural health monitoring, *Structural Health Monitoring, 1,* 1-12.

16. Machado, M. R., Santos, J. (2015). Reliability analysis of damaged beam spectral element with parameter uncertainties. *Shock and Vibration*.

17. Machado, M., Adhikari, S., Santos, J. (2017). A spectral approach for damage quantification in stochastic dynamic systems, *Mechanical Systems and Signal Processing, 88,* 253-278.

18. Clough, R., Penzien, J. (1993). *Dynamics of structures*. McGraw Hill, New York.

19. Yu, B. Y. J., Soliman, M. (2014). Estimation of cable tension force independent of complex boundary conditions. *ASCE Journal of Engineering Mechanics, 60,*1-8.

20. Rao, S. S. (2008). *Mechanical vibration.* Person Prentice-Hal.

21. Dutkiewicz, M., Machado, M. R. (2019a). Spectral approach in vibrations of overhead transmission lines. *IOP Conference. Series: Materials Science and Engineering, 471,* 052029.

22. Dutkiewicz, M., Machado, M. R. (2019b). Dynamical response of overhead transmission line in turbulent wind flow with application of the Spectral Element Method. *IOP Conference Series: Materials Science and Engineering, 471,* 052031.

23. Doyle, J. F. (1997). Wave propagation in structures: spectral analysis using fast discrete fourier transforms, 2nd Edition. *Mechanical engineering.* Springer-Verlag New York, Inc., New York.

24. Zienkiewicz, O. C., Taylor, R. L. (1991). *The finite element method*, 4th Edition. McGraw-Hill, London.

25. American Institute of Aeronautics and Astronautics (AIAA) (1998). Guide for the verification and validation of computational fluid dynamics simulations. *Technical Report No. AIAA-G-077-1998.*

26. American Society of Mechanical Engineers (ASME) (2006). Guide for the verification and validation in computational solid mechanics. *Technical Report No. ASME V&V 10-2006.*

27. Oberkampf, W. L., Trucano, T. G. (2002). Verification and validation in computational fluid dynamics. *Progress in Aerospace Sciences, 8,* 209-272.

28. Aeschliman, D. P., Oberkampf, W. L., Blottner, F. G. (1995). A Proposed Methodology for CFD Code Verification, Calibration, and Validation, Paper 95-CH3482-7. *16th International Congress on Instrumentation for Aerospace Simulation Facilities*.

29. Schwer, L. E. (2007). Validation metrics for response histories: perspectives and case study. *Engineering with Computers, 23,* 295-309.

30. William, L., Oberkampf, W. L., Smith, B. (2014). Assessment criteria for computational fluid dynamics validation benchmark experiments. *52nd Aerospace Sciences Meeting*.

31. William, L., Oberkampf, W. L., Barone, M. F. (2006). Measures of agreement between computation and experiment: validation metrics. *Journal of Computational Physics, 217,* 5-36.

32. Russell, D. M. (1997). Error measures for comparing transient data: part I: development of a comprehensive error measure. *Proceedings of the 68th shock and vibration symposium,* 175-184.

33. Geers, T. L. (1984). An objective error measure for the comparison of calculated and measured transient response histories. *Shock Vib Bull, 54,* 99-107.

34. Aeschliman, D. P., Oberkampf, W. L. (1998). Experimental methodology for computational fluid dynamics code validation. *AIAA Journal, 36, 5,* 733-741.

35. Barber, T. J. (1998). Role of code validation and certification in the design environment. *AIAA Journal, 36, 5,* 752-758.

36. Benek, J. A., Kraft, E. M., Lauer, R. F. (1998). Validation Issues for Engine-Airframe Integration. *AIAA Journal, 36, 5,* 759-764.

37. Bertin, J. J., Martellucci, A., Neumann, R. D., Stetson, K. F. (1993). Developing a data base 94 for the calibration and validation of hypersonic CFD codes-sharp cones. AIAA Paper No. 93-3044. *24th AIAA Fluid Dynamics Conference*.

38. Bradley, R. G. (1988). CFD Validation Philosophy, AGARD-CP-437. *Fluid Dynamics Panel Symposium: Validation of Computational Fluid Dynamics*, Lisbon, Portugal.

39. Coleman, H. W., Stern, F. (1997). Uncertainties and CFD Code Validation. *Journal of Fluids Engineering, 119,* 795-803.

40. Mehta, U. B. (1996). Guide to credible computer simulations of fluid flows. *Journal of Propulsion and Power, 12(5),* 940-948.

41. Sprague, M. A., Geers, T. L. (2003). Spectral elements and field separation for an acoustic fluid subject to cavitation. *Journal of Computational Physics, 181,*149-162.

42. Den Hartog, J. P. (1932). Transmission line vibration due to sleet. *Transactions of the American Institute of Electrical Engineers, 51(4),* 1074-1086.